Hindawi
Journal of Nanomaterials
Volume 2022, Article ID 6478781, 11 pages
https://doi.org/10.1155/2022/6478781

Research Article

Tribological Characteristics of GCI-EN31 Steel Surface Contact with Dry Sliding Condition

S. Ananth,[1] **P. Sivaprakasam**,[2] **J. Udaya Prakash**,[3] **B. Ravi**,[4] **G. Kalusuraman**,[5] **and R. Sundarakannan**[6]

[1]*Department of Mechanical Engineering, Vardhaman College of Engineering, Shamshabad, Hyderabad, Telangana, India*
[2]*Department of Mechanical Engineering, College of Electrical and Mechanical Engineering, Addis Ababa Science and Technology University, Addis Ababa, Ethiopia*
[3]*Department of Mechanical Engineering, Vel Tech Rangarajan Dr. Sagunthala R&D Institute of Science and Technology, Chennai, Tamil Nadu, India*
[4]*Department of Mechanical Engineering, Swarna Bharathi Institute of Science and Technology, Khammam, Telangana, India*
[5]*Department of Agricultural Engineering, Kalasalingam Academy of Research and Education, Krishnankoil, Tamil Nadu, India*
[6]*Institute of Agricultural Engineering, Saveetha School of Engineering, SIMATS, Chennai, Tamil Nadu, India*

Correspondence should be addressed to P. Sivaprakasam; shiva@aastu.edu.et

Received 19 March 2022; Accepted 22 April 2022; Published 11 May 2022

Academic Editor: V. Vijayan

Grey cast iron (GCI) and steel contact surface application is an inevitable component and provides good wear resistance in several applications, not only in automobiles. Grey cast iron consists of a predominantly pearlitic/ferrite matrix or both with graphite flakes. The majority of previous research works were based on three different types of wear regimes. The wear regimes enumerate the wear track morphology, wear rate, and COF of the respective application. In this research work, dry sliding wear properties of GCI and EN31 pins were examined with different sliding parameters using pin on disc wear test. The weight loss, coefficient of frictions, and surface morphology were considered for experimental analysis. Due to the transfer of wear debris from the GCI disc, the counter steel pin surface experienced a progressive reduction in wear with increasing speed and load. With 30 N and 45 N contact loads and sliding speeds up to 1 m/sec, the GCI shows marginally positive wear. The surface textures were analyzed with the help of SEM and a surface roughness tester.

1. Introduction

Loss of material due to friction was encountered more often between two contact surfaces. Wear is the most commonly encountered in prime movers, particularly due to adhesion, leading to frequent replacement of components [1]. During dry sliding conditions, the observed wear normal modes are plowing, mild, and oxidative wear. This includes useful run-in wear as well. Adhesive wear is usually described as material transfer between two surfaces. Surface-to-surface contact, even though lubricated, can occur if the lubricant film has a discontinuity, resulting in material transfer and surface damage. Cold welding takes place in dry sliding wear between two surfaces, with one of the surfaces releasing small particles which build up or agglomerate and transfer to another surface in layers. These built-up edges can be seen in cutting tools. Grey iron is used in a variety of engineering applications, including diesel engine components such as cylinder heads, piston rings, and engine blocks, where wear is a significant factor when using wet lubrication. Grey cast iron's properties are highly dependent on the graphite morphology and volume fraction (H. Mohamadzadeh et al., [2]). Response surface methodology was used to optimize the composites' tribological behaviour. According to the optimization results, the content of seashell powders increased the wear and frictional resistance of the composites, and it was the most influential factor (V. Bhuvaneswari et al.,[3]). The ball on disc sliding wear test was used to investigate the

tribological behaviour of the alumina coating. The alumina coating was shown to reduce the COF value and wear mass loss of the GCI substrate by at least ten percent and fifty percent, respectively [4]. Wear and scratch tests revealed that EN 36C steel coated with 75: 25 YSZ-Al2O3 exhibits superior wear and scratch resistance when compared to the other materials [5]. A. Saravanakumar et al., [6] investigated the wear characteristics of aluminium alloy AA2219-graphite (Gr) composites in dry sliding conditions. The effect of the initial deflection angle (IDA) on the tribological properties of grey cast iron (GCI) rings with curve distributed pits in the radial direction is investigated in this study (CDPRD). The antiwear performance of samples was determined using a pin-on-disc wear test rig with a normal load of 70 N and a rotating speed of 200 rpm [7].

Austempered grey cast iron is a material with solid, light, and wear-resistant qualities. It is also a good material for high design and production adaptability, as well as being cost effective [8]. Due to its high friction coefficient, low cost, good damping property, fine castability, machinability, and other properties, grey cast iron (GCI) is one of the most commonly used materials in industrial applications (N. Sun et al., [9]). According to literature surveys [10], a small amount of free ferrite is dispersed in the region of perlite matrix. Such a matrix composition provides good wear resistance between the two sliding surfaces and in similar applications like brakes, cylinder liners, and piston rings. Another investigation describes the association of two distinct regions of grey pearlitic cast iron that were exposed during the dry sliding wear experimentation [11, 12]. In the initial region of the crystal structure, the graphite dominates to mitigate the wear rate, and its graph has linear correlation. In the consequent portion crystal region, the loss of material due to friction was driven by two thermally simulated processes, namely, in the first case, the phenolic binder was degraded thermally, and in the next case, it was driven by tribooxidation. In the second case, specific wear rate was found to be better. Ghaderi et al. [13] examined three different materials of cast iron, including nodular, grey, and condensed iron, with different chemical conformations and subjected them to austempering (process carried out at 350°C). The investigation extended to find knowledge regarding graphite morphology and comparison with the pearlitic grey iron tested with the help of a block-on-ring wear tester. Austempered nodular iron shows high impact test results compared to austempered grey iron. Cast iron and Compacted Graphite Iron revealed higher wear resistance than other types of cast iron and lower wear resistance and lower impact test results due to the presence of graphite in the microstructure.

In the dry condition of surface contact, the normal wear that occurs in GCI is quite high, and the same was stated by Chawla et al. [14] in their experimentation. At an increasing sliding speed, wear was attributed more to stainless steel, and it was softened during its increasing load factor. It is vice versa in the case of GCI, and it happened due to the existence of graphite (ferrite), and decohesion was observed.

Cho et al. [15] observed the loss of material due to the sliding properties of grey iron by changing the carbon equivalent (CE). On all speeds of experimentation, the GCI of flake graphite dominates good wear resistance. On the other hand, the ferrite of GCI shows no change in coefficient of friction. Hirasata et al. [16] observed the wear rate, COF, and hardness in various ranges of cast iron under heavy range conditions. At the beginning stage of sliding distance, the hardness and COF show a lower hardness with a huge loss of material due to friction, and in the later stage of high sliding speed, there is a less amount of material loss due to the presence of stable graphite particles.

Wilson et al. [17] observed the reduced wear due to the influence of oxide particles and suggested another important oxidative wear model. Liu et al. [18] evaluated the hardness properties and variation of carbide grains due to the effect of shakeout time during the solidification process and found that at high hardness and strength, the cast iron shows increased wear rate due to oxidation. R. M. Galagali et al., [19] investigated the wear behaviour of austempered ductile iron against temperature and sliding speed. The wear rate was high up to a sliding speed of 2 m/s but significantly decreased above that speed. There is a work hardening effect at room temperature caused by the conversion of the remaining austenite to martensite. This makes the metal more durable. As with elevated temperatures, a constant rate of wear was observed with a dry sliding condition that increased significantly with speed. The temperature of the hands combined with the sliding speed has a greater effect on the rate of wear. Surface texturing of grey cast iron using femtosecond pulse duration improved wear resistance compared to untextured, millisecond, and nanosecond laser-textured surfaces [20]. Surface texturing research has exploded in recent years to improve lubrication in tribological applications [21]. The research activities in the field of tribology have grown rapidly in various sectors, in terms of both scope and depth recently, according to Meng et al. [22]. Despite its good features, it must withstand application settings such as dry and lubricated sliding, which have

Table 1: Process parameter and their levels.

Levels	Parameters		
	Load L (N)	Sliding speed, S (m/s)	Sliding distance, D (m)
1	15	0.5	300
2	30	1	600
3	45	1.5	900

Figure 1: Pin-on-disc set-up used for dry sliding test.

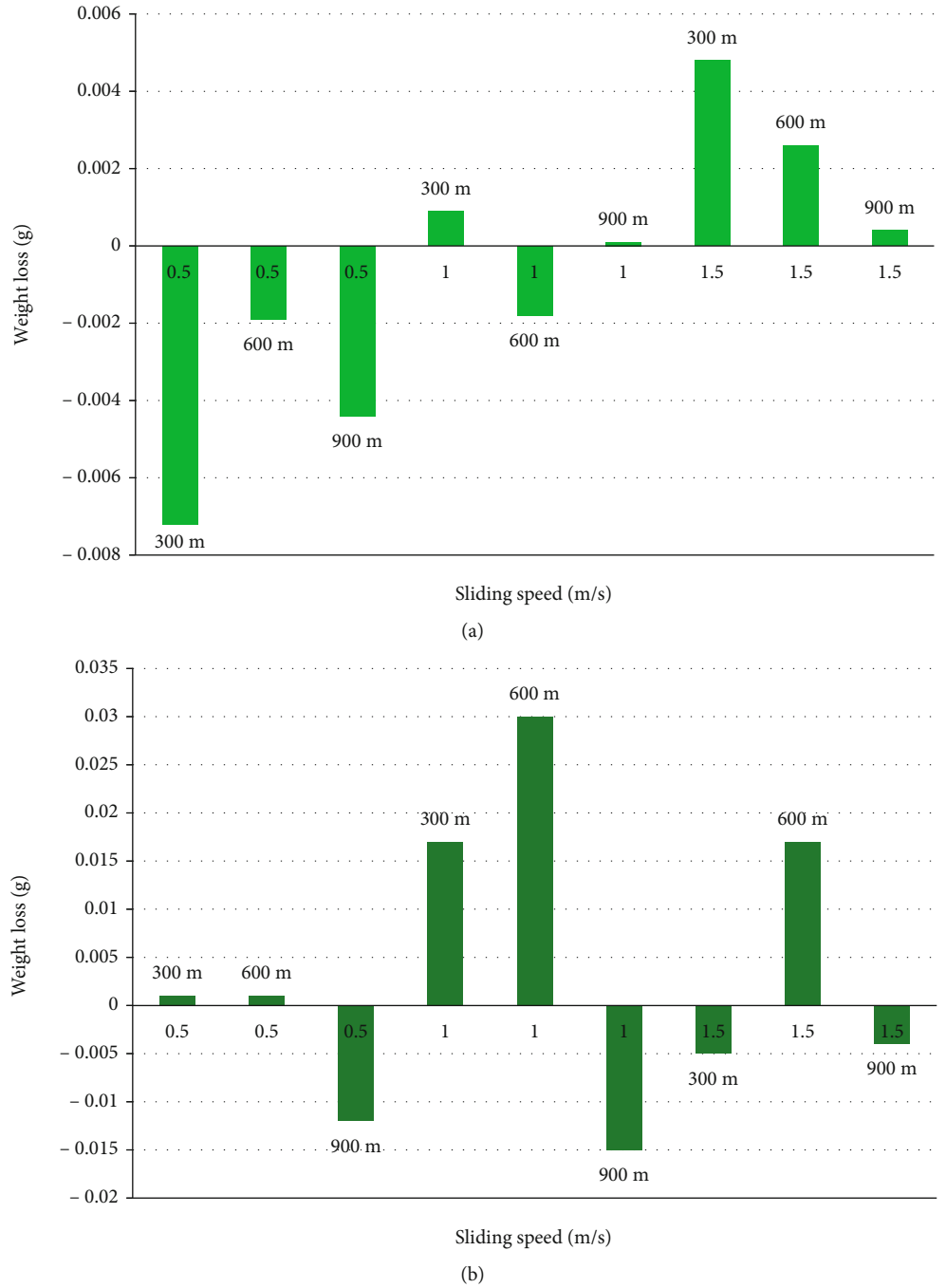

Figure 2: (a) Disc weight loss at 15 N and (b) pin weight loss at 15 N.

exposed positive and negative wear. Many researchers have tried to find out how grey cast iron wears. Only a few studies have talked about both the positive and negative wear behaviour of GCI.

2. Experimental Procedure

2.1. Sample Preparation and Test Parameters. In this experimentation, EN-31 is the counterpart material, and standard GCI test samples were machined to conduct the experiments [23]. Wear tests were carried out at three different parameters, and their levels are shown in Table 1. The test samples were prepared and experimented on the basis of the Taguchi Design of Experiment (DOE) with an Orthogonal Array (OA) of L_{27}.

2.2. Dry Wear Test. The wear test that is to be conducted in a normal atmospheric environment, and without lubrication is known as the "dry sliding wear test." The pin-on-disc set-up used for experiments with dry sliding wear tests is shown in Figure 1. The sliding wear experiments were carried out under dry sliding conditions at room temperature

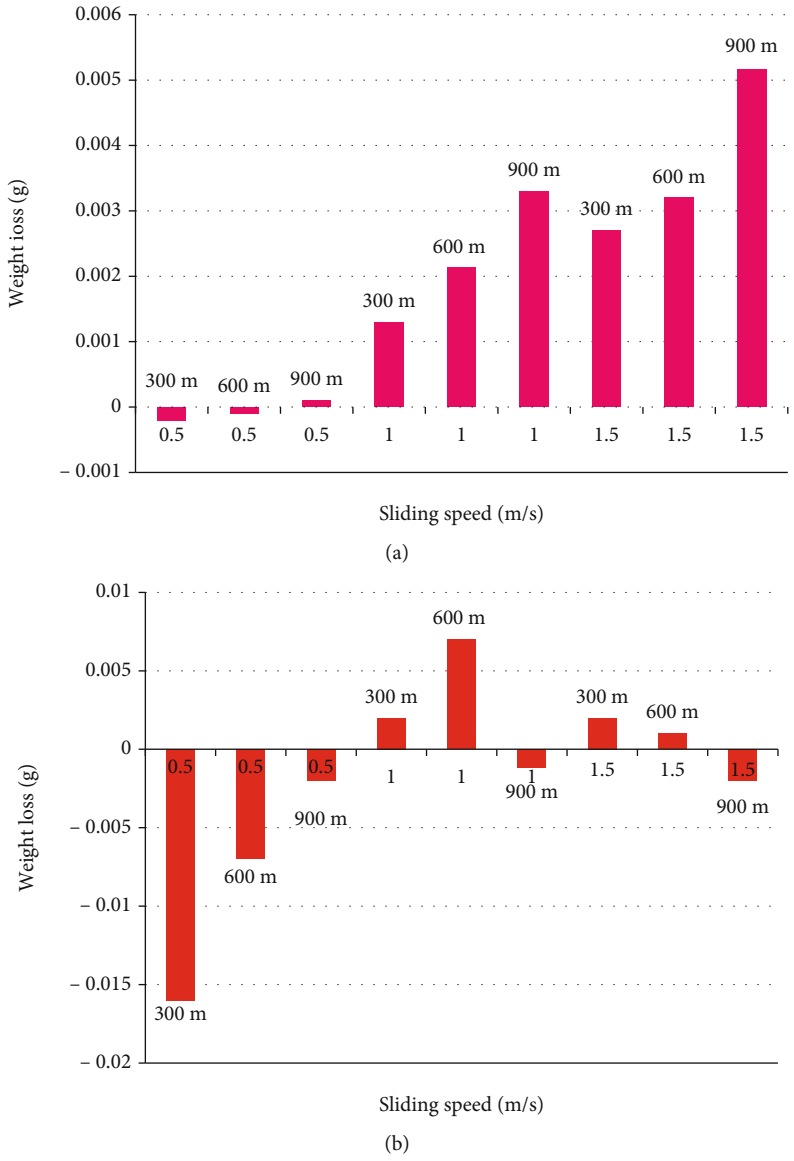

Figure 3: (a) Disc weight loss at 30 N and (b) pin weight loss 30 N.

in compliance with the ASTM standard G 99 [24, 25]. The EN31 pin was thoroughly cleaned using acetone. A pin was clamped at one end of the cantilever beam in a slot and tightened with the help of a screw. The cleaned disc specimen of grey cast iron was loaded on top of the circular column and tightened. To set the wear track on the disc, the pin was positioned over the disc at a 15 mm radius from the centre of the disc material.

The required weight was placed on the loading pan at the other end of the cantilever beam slowly without shaking. The wear test was started by pressing the push button on the controller panel. The necessary test parameter readings like coefficient of friction, speed, and load were noted and repeated the procedure for a suitable combination for the next test condition. The experiments were carried out on GCI discs with an outer diameter of 55 mm, an inner diameter of 6 mm, and a thickness of 10 mm. GCI has a surface hardness of 28 HRC. The counter specimen pin EN31 was made of BS 970 steel and has a diameter of 6 mm and a length of 60 mm. Totally 27 experimental combination were performed using Taguchi-based design on experiments. The weights of pin and disc for each experiment before and after wear test measured using precision weighing machine.

3. Result and Discussion

3.1. Dry Slide Wear Study. Sliding wear tests have been conducted in a dry environment, and the test results are discussed as follows. Normally, the response of the contact surface under dry sliding depends on the material dependence PV (pressure P and sliding velocity V) factor. With increasing PV, the contact interface will be exposed to a rise in temperature and, accordingly, thermally influenced wear response will occur. Also, with heterogeneous structures such as CI, this response is more complex. This leads to

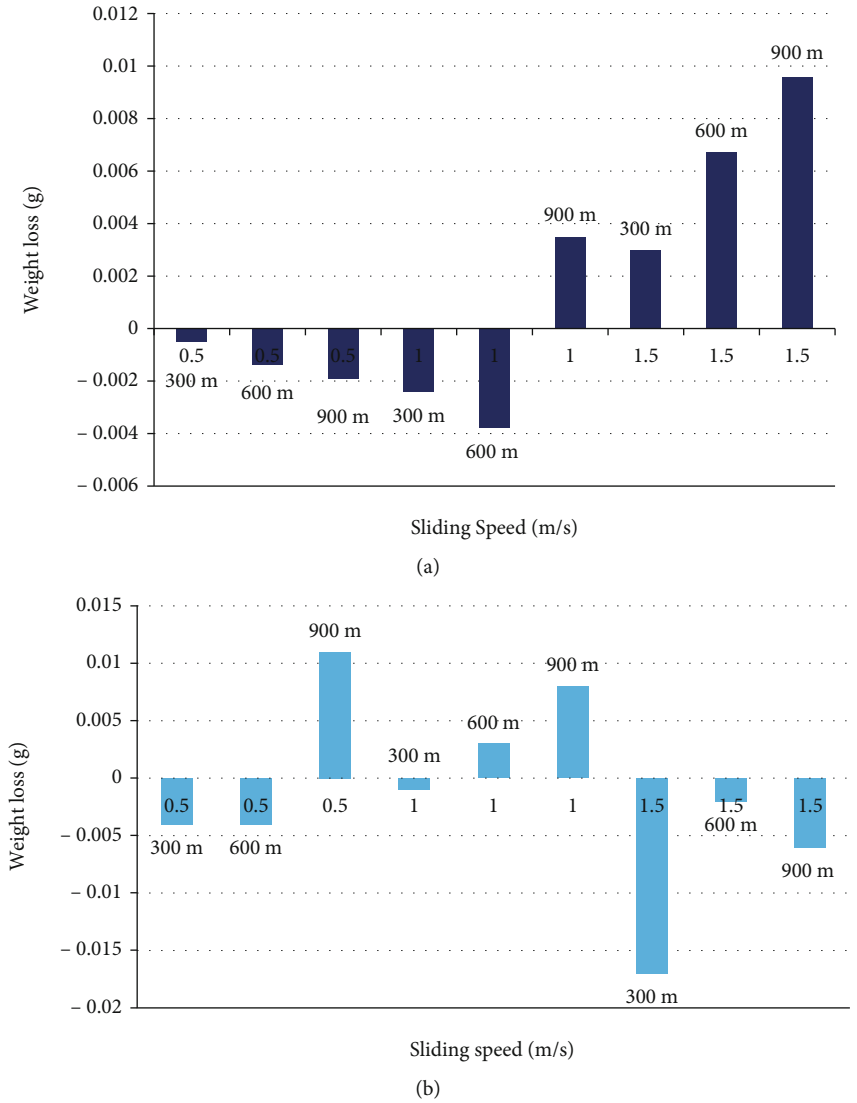

Figure 4: (a) Disc weight loss at 45 N and (b) pin weight loss at 45 N.

material transfer between contacting surfaces, resulting in condition-dependent –ve and +ve modes of wear.

Observation with 15 N with various sliding speeds and distances shows that while the GCI disc tends to display a reduced order of wear (due to run-in), the counter steel (pin) surface tends to show –ve approach of wear (alter suitable to transfer of wear particles) with 30 N and 45 N and both the CI disc and counter pin exhibit an increasing order of wear attributable to the significance of the PVT factor on wear.

Figure 2(a) describes the wear that occurs in both positive and negative modes with increasing sliding speed and sliding distance under a load of 15 N for the GCI disc. Figure 2(b) explains the variation of wear with increasing sliding speed and distance under load of 15 N for EN31 steel pins.

From Figure 2(a), it is evident that the GCI disc exhibits the negative wear at lower sliding speed. The wear tends to positive mode while at a sliding speed of 1 m/sec to 1.5 m/sec. It has been found that at low sliding speeds, the negative mode of wear happens. At medium and high sliding speeds, mostly positive mode of wear has been found. The typical variation of wear of the counter steel surface at 15 N load is observed in Figure 2(b). Compared to the GCI wear track, the steel pin encounters relatively higher order wear. Mostly positive kinds of wear are observed. The observation of a +ve mode of wear for both the GCI disc and steel pin suggests little material transfer between the contacting surfaces.

Figures 3(a) and 3(b) show that with a 30 N load, the GCI disc has the least wear at 0.5 m/sec and tends to increase wear while sliding speed and distance (+ve mode). Whereas the counter steel pin's wear track begins in negative mode and tends to increase to positive mode (+ve mode) with increasing speed (i.e., greater sliding distance at 900 m), it may drop down (-ve mode), causing the graphite flakes of cast ion to be shifted to the steel's surface, resulting in the observed –ve wear.

Figure 4(a) implies that the GCI disc exhibits mild –ve wear with lower sliding velocity (0.5 m/sec) and up to 600 m of sliding distance with 1 m/sec. Then, it tends to

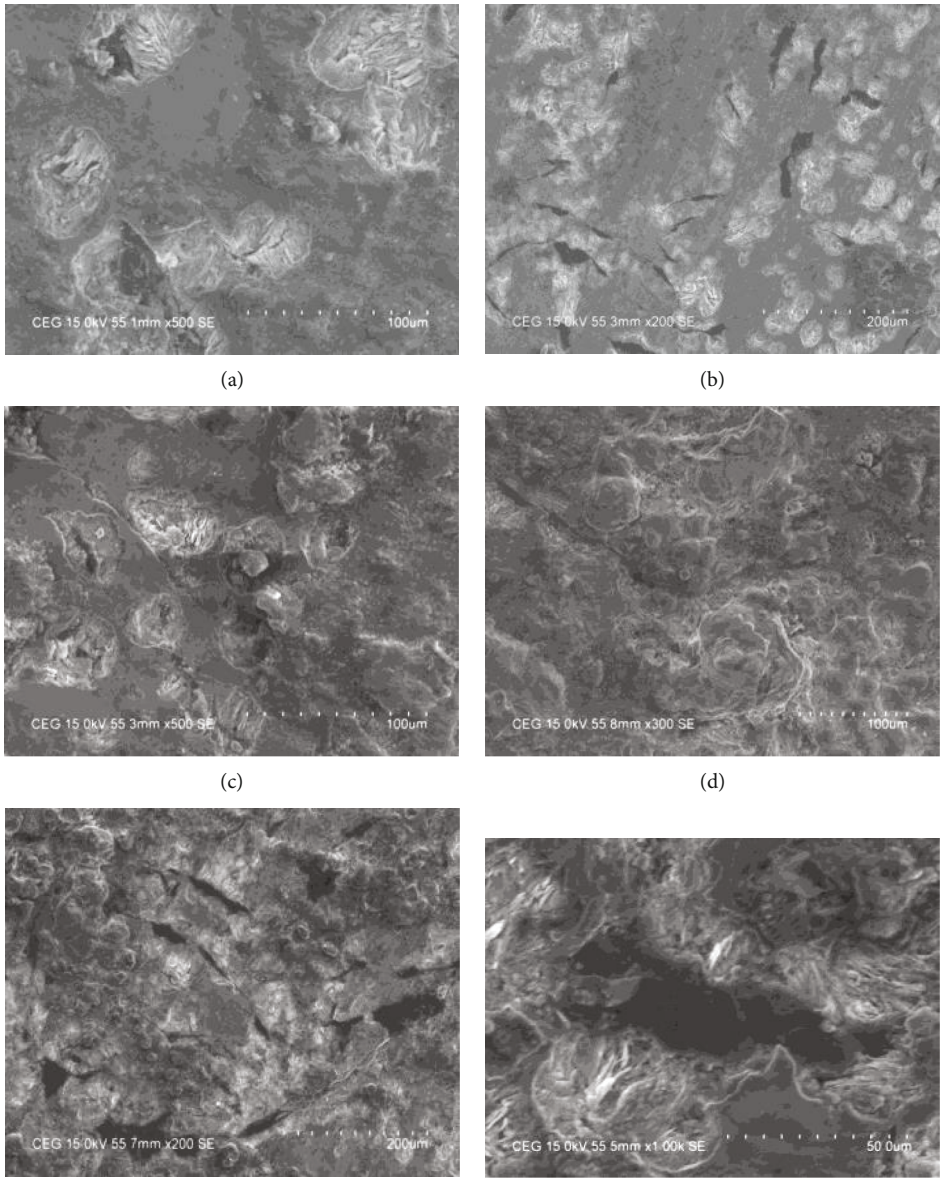

Figure 5: (a–f) Micrograph with dry sliding with 15 N load.

change its wear from –ve to +ve mode (it is known that normal GCI contains graphite, a layer lattice material, which on sliding contact pressure undergoes interplaner shear, forming a solid lubricant film for sliding). This is facilitated mostly with increased sliding speed and duration (distance traversed-PVT factor).

The typical wear of the counterpart (pin) surface is shown in Figure 4(b). It is seen that the pin surface exhibits mostly +ve modes of wear (fluctuation) with a dominant –ve mode of wear at higher contact load and sliding speed. Due to contact temperature, the steel surface would be oxidized, and there could also be unstable oxide film growth, and hence, the steel surface undergoes a fluctuating +ve mode of wear. However, with a higher sliding speed (1.5 m/sec), the transfer of graphite from GCI results in the observed –ve mode of wear.

3.2. SEM Observation. Figure 5(a) shows the contribution of material debris transfer for both the surface and the load of 15 N for the worn out portion of the GCI disc wear track. Discrete transfers of wear debris take place from the counter steel surface. Figure 5(b) shows how the GCI track is ploughed with dominant slide bands. The debris on the steel surface and how it is spread over the surface can be seen. Figure 5(c) depicts the graphite layer detaching and the transfer of steel surface debris embedded in the graphite flake.

A micrograph of the worn out GCI track under dry sliding with a 15 N load, 1.5 m/sec sliding speed, and a transverse distance of 900 m is shown in Figure 5(d). The micrograph depicts discrete pull out of graphite with the absence of any transferred particles (+ve mode of wear). The micrograph's worn out GCI track (Figure 5(e)) shows

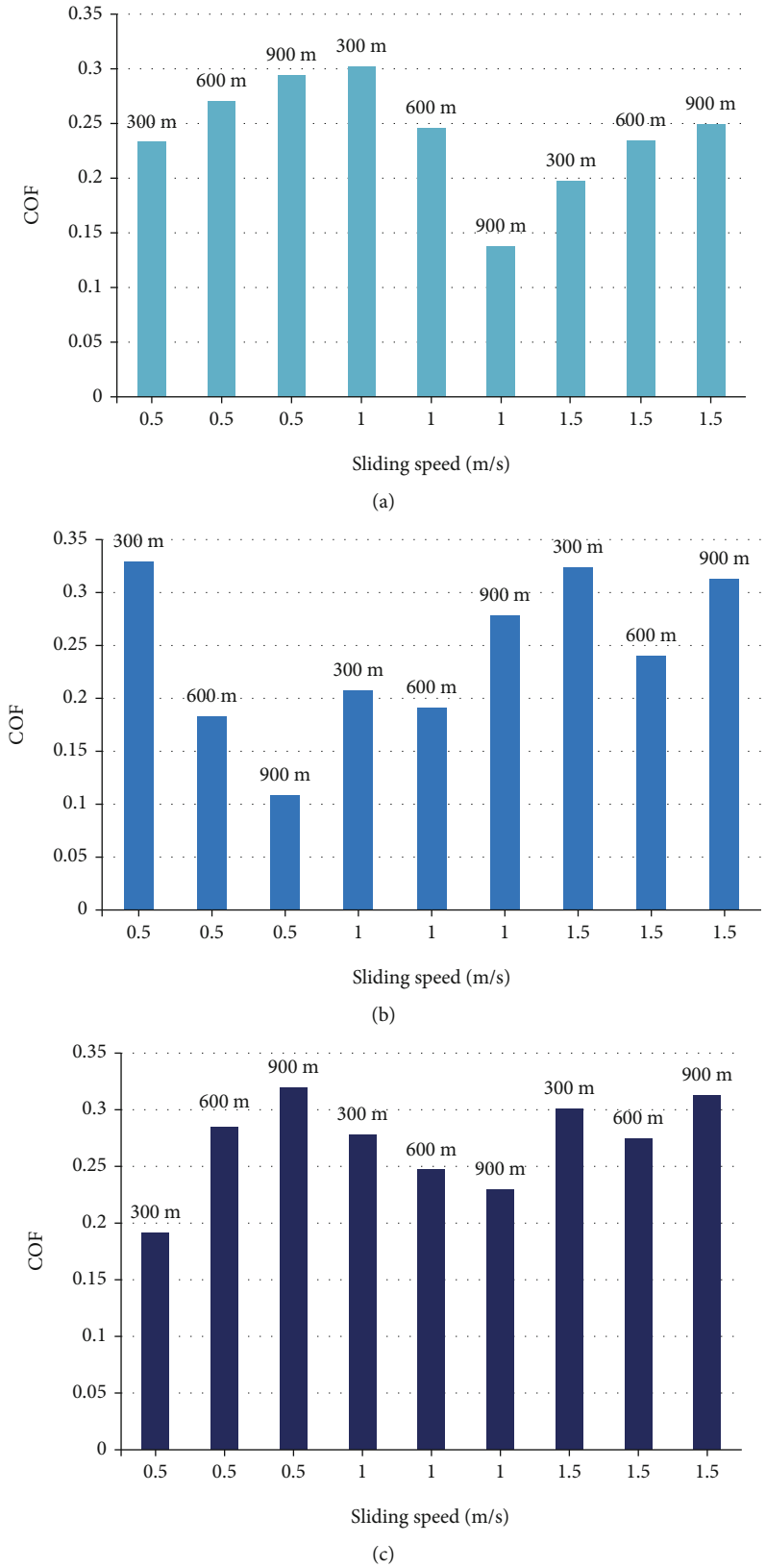

Figure 6: (a) Disc COF at 15 N, (b) disc COF at 30 N, and (c) disc COF at 45 N.

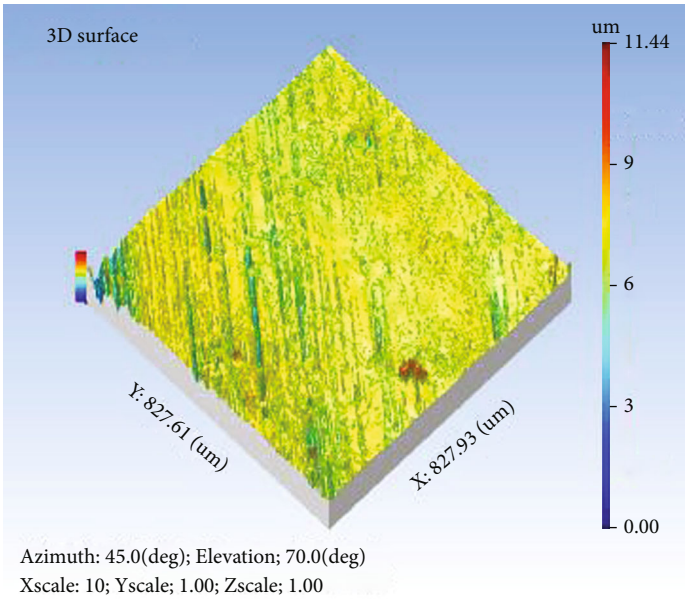

(a) 15 N, 1.5 m/sec, 900 m

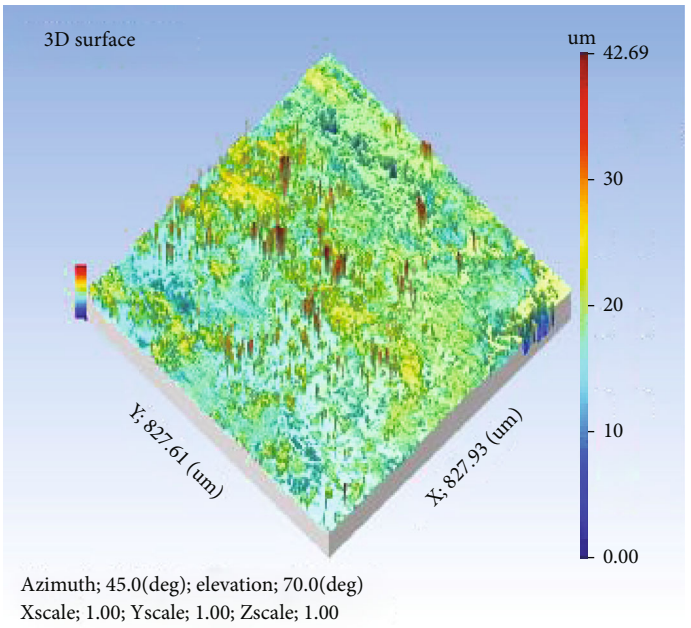

(b) 30 N, 1.5 m/sec, 900 m

Figure 7: Continued.

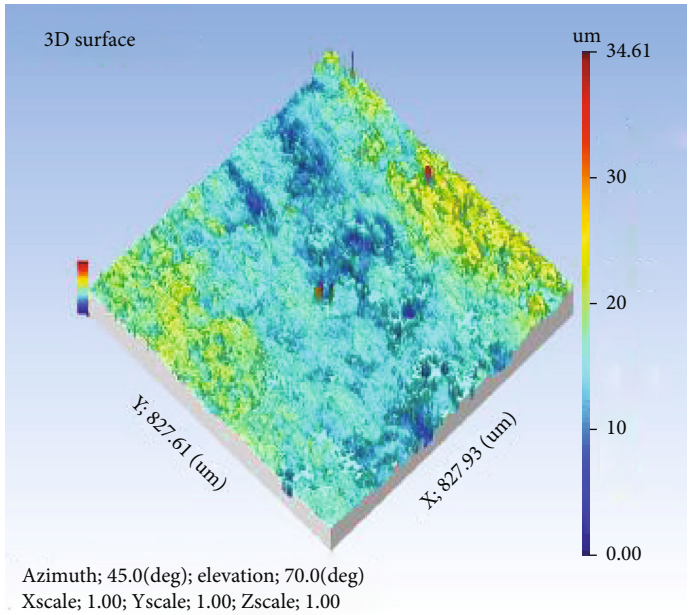

(c) 45 N, 1.5 m/sec, 900 m

Figure 7: (a-c) 3D surface images.

flow of surface material with discrete ridges and surface cracks. Figure 5(d) depicts a micrograph of the worn out GCI track surface exhibiting discrete cleavage/surface fissures next portion of the worn out track describes the observation of the worn out transferred portion on GCI. The graphite layer is partly unpeeled, whereas ferrite structure exposed on substrate. Figure 5(f) depicts graphite flaking, revealing the texture beneath the ferrite structure.

3.3. Coefficient of Friction (COF). The typical observed variation of COF, with sliding speed at 15 N load, is illustrated in Figure 6(a). It is seen that with a lower speed of 0.5 m/sec, COF increases while increasing sliding distance. A mild rise in COF observed at the speed of sliding (1 m/sec) with a lower sliding distance of 300 m could be attributed to less transfer of graphite. The COF was reduced in (trials 5 and 6) with sliding speed of 1 m/sec and a sliding distance of 600 m and 900 m and a sliding speed of 1.5 m/sec and a sliding distance of 300 m, 600 m, and 900 m. The reason for the reduction in COF could be attributed to the transfer of graphite film.

The variation of COF in dry sliding with a load of 30 N is demonstrated in Figure 6(b). It is witnessed that COF drops down, which is attributed to the change for ploughing sliding. With increasing speed, a gradual increase of COF is observed. This may be attributed to increased contact area and interaction on account of higher speed/loads. Figure 6(c) depicts the variation of COF with sliding condition at 45 N load. The COF varied from 0.194 to 0.319, indicating relatively steadier sliding at 0.5 m/sec. It is seen that with sliding speeds of 1 m/sec and 1.5 m/sec, there is variation in COF. This could be attributed to increased contact area and consequent interaction. With a higher sliding speed of 1.5 m/sec, the observed marginal variation in COF could be attributed to steadier sliding.

3.4. Surface Roughness. Figure 7(a) shows the 3D surface of the worn surface presents no visible lay pattern. In this case, positive wear mode appeared with a 15 N load, a 1.5 m/sec sliding speed, and 900 m sliding distance. The roughness parameters of this surface have Ra 0.182 μm, Rt 2.31 μm, and Rt/Ra > 10. It has been discovered that the mild crest flattened texture exists. Kurtosis is 26.1, and skewness is -2.54. Fine surface roughness values 180 nm were observed; also, there were no sticking and adhesion of another materials.

Figure 7(b) depicts the 3D surface with a 30 N load, a sliding speed of 1.5 m/sec, and a sliding distance of 900 m. The texture on a 3D surface is random, with no discernible lay pattern. The roughness parameters of this surface have Ra 1.70 μm, Rt 24.5 μm,Rt/Ra > 10, Rp 10.8 μm, and Rv 2.97 μm. Kurtosis is 14.3, and skewness is -1.29. An absence of crest flattening has been observed in a highly random and noncentric profile. It shows that more rough texture compared to load 15 N, and it has found that materials deposited on surfaces. At higher loads, more amounts of materials transformed between the materials and produced coarse surfaces. Figure 7(c) shows the 3D surface at 45 N load, 1.5 m/sec sliding speed, and 900 m sliding distance. The r. The roughness parameters of this surface have Ra 1.37 μm, Rt 15.8 μm,Rt/Ra > 10, kurtosis 4.38, skewness -0.45, mild wavy texture, and left centric profile.

4. Conclusions

Under dry sliding conditions, the GCI disc exhibits an increase in wear with increasing load. The counter steel pin

surface experienced a progressive reduction in wear with increasing speed and load, attributable to the transfer of wear debris from the GCI disc. The GCI exhibits marginal +ve wear with 30 N and 45 N contact load and sliding speeds of up to 1 m/sec. A micrograph of the worn out track of a GCI disc reveals the transfer of worn out debris (20 to 40 μm), from steel surface.

With a 15 N load, the COF increases while increasing the sliding distance at low and high levels of sliding speed, whereas at a medium sliding speed of 1 m/sec, it decreases from a higher to a lower value, indicating a transition from sliding form ploughing to stable mode. A mild rise in COF was observed at a higher speed of sliding (1 m/sec), attributable to less transfer of graphite.

The COF drops down initially at 30 N, lower sliding speeds, and with increasing speed, and a gradual increase of COF was observed. This may be attributable to an increase in contact area and interaction on account of higher speeds/loads.

At lower speeds, with a 45 N load, the COF is relatively steady, but at higher speeds, the COF gradually increases with increasing sliding speed.

At 15 N load, with a low initial stage of distance and sliding speed, the worn out surface presents an unsystematic surface texture with Ra 0.136 μm, while with medium speed of 1 m/sec, it presents a coarse texture with Ra value of 0.398 μm. At higher levels of sliding speed and distance, a mild wavy texture (Ra 1.37 μm) and a left centric profile were detected.

Data Availability

The data used to support the findings of this study are included within the article.

Conflicts of Interest

The authors declare that they have no conflicts of interest regarding the publication.

References

[1] A. Renz, D. Kürten, and O. Lehmann, "Wear of hardfaced valve spindles in highly loaded stationary lean-burn large bore gas engines," *Wear*, vol. 376-377, pp. 1652–1661, 2017.

[2] H. Mohamadzadeh, H. Saghafian, and S. Kheirandish, "Sliding wear behavior of a grey cast iron surface remelted by TIG," *Journal of Materials Science and Technology*, vol. 25, no. 5, pp. 622–628, 2009.

[3] V. Bhuvaneswari, L. Rajeshkumar, and K. N. S. Ross, "Influence of bioceramic reinforcement on tribological behaviour of aluminium alloy metal matrix composites: experimental study and analysis," *Journal of Materials Research and Technology*, vol. 15, pp. 2802–2819, 2021.

[4] Z. A. Abd Halim, N. Ahmad, M. F. Hanapi, and M. F. Zainal, "Rapid surface treatment of grey cast iron for reduction of friction and wear by alumina coating using gas tunnel plasma spray," *Materials Chemistry and Physics*, vol. 260, article 124134, 2021.

[5] M. Ramesh, K. Marimuthu, P. Karuppuswamy, and L. Rajeshkumar, "Microstructure and properties of YSZ-Al2O3 functional ceramic thermal barrier coatings for military applications," *Boletin de la Sociedad Espanola de Ceramica y Vidrio*, 2021.

[6] A. Saravanakumar, L. Rajeshkumar, D. Balaji, and M. P. Jithin Karunan, "Prediction of wear characteristics of AA2219-Gr matrix composites using GRNN and Taguchi-based approach," *Arabian Journal for Science and Engineering*, vol. 45, no. 11, pp. 9549–9557, 2020.

[7] S. Sun, R. Long, Y. Zhang, and M. Li, "The influence of initial deflection angle on the tribological properties of gray cast iron rings with curve distributed pits under dry sliding," *Proceedings of the Institution of Mechanical Engineers, Part J: Journal of Engineering Tribology*, vol. 235, no. 8, pp. 1659–1668, 2021.

[8] S. K. Putatunda, "Austempering of silicon manganese cast steel," *Materials and Manufacturing Processes*, vol. 16, no. 6, pp. 743–762, 2001.

[9] N. Sun, H. Shan, H. Zhou et al., "Friction and wear behaviors of compacted graphite iron with different biomimetic units fabricated by laser cladding," *Applied Surface Science*, vol. 258, no. 19, pp. 7699–7706, 2012.

[10] V. Nayyar, J. Kaminski, A. Kinnander, and L. Nyborg, "An experimental investigation of machinability of graphitic cast iron grades; flake, compacted and spheroidal graphite iron in continuous machining operations," *Procedia CIRP*, vol. 1, pp. 488–493, 2012.

[11] G. Straffelini and L. Maines, "The relationship between wear of semi metallic friction materials and pearlitic cast iron in dry sliding," *Wear*, vol. 307, no. 1-2, pp. 75–80, 2013.

[12] E. E. Vera-Cardenas, R. Lewis, and T. Slatter, "'Sliding wear study on the valve-seat insert contact', Open," *Journal of Applied Sciences*, vol. 7, no. 2, pp. 42–49, 2017.

[13] A. R. Ghaderi, M. N. Ahmadabadi, and H. M. Ghasemi, "Effect of graphite morphologies on the tribological behavior of austempered cast iron," *Wear*, vol. 255, no. 1-6, pp. 410–416, 2003.

[14] K. Chawla, N. Saini, and R. Dhiman, "Investigation of tribological behavior of stainless steel 304 and gray cast iron rotating against EN32 steel using pin on disc apparatus," *IOSR Journal of Mechanical and Civil Engineering (IOSR-JMCE)*, vol. 9, no. 4, pp. 18–22, 2013.

[15] M. H. Cho, S. J. Kim, R. H. Basch, J. W. Fash, and H. Jang, "Tribological study of gray cast iron with automotive brake linings: the effect of rotor microstructure," *Tribology International*, vol. 36, no. 7, pp. 537–545, 2003.

[16] K. Hirasata, K. Hayashi, and Y. Inamoto, "Friction and wear of several kinds of cast irons under severe sliding conditions," *Wear*, vol. 263, no. 1-6, pp. 790–800, 2007.

[17] J. E. Wilson, F. H. Stott, and G. C. Wood, "The development of wear protective oxides and their influence on sliding friction," *Proceedings of the Royal Society of London. A. Mathematical and Physical Sciences*, vol. 369, no. 1739, pp. 557–574, 1980.

[18] Y. C. Liu, J. M. Schissler, and T. G. Mathia, "The influence of surface oxidation on the wear resistance of cast iron," *Tribology International*, vol. 28, no. 7, pp. 433–438, 1995.

[19] R. M. Galagali, M. H. Ashok, V. M. Khadakbhavi, J. Shivakumar, S. Malagi, and C. Patil, "Effect of speed and temperature on the tribological behaviour of ADI," in *Recent Advances in Mechanical Infrastructure. Lecture Notes in Intelligent Transportation and Infrastructure*, A. K. Parwani, P.

Ramkumar, K. Abhishek, and S. K. Yadav, Eds., Springer, Singapore, 2022.

[20] R. Bathe, V. Sai Krishna, S. K. Nikumb, and G. Padmanabham, "Laser surface texturing of gray cast iron for improving tribological behavior," *Applied Physics A: Materials Science & Processing*, vol. 117, no. 1, pp. 117–123, 2014.

[21] L. R. R. da Silva and H. L. Costa, "Tribological behavior of gray cast iron textured by maskless electrochemical texturing," *Wear*, vol. 376-377, pp. 1601–1610, 2017.

[22] Y. Meng, J. Xu, Z. Jin, B. Prakash, and Y. Hu, "A review of recent advances in tribology," *Friction*, vol. 8, no. 2, pp. 221–300, 2020.

[23] S. Ananth, P. Sivaprakasam, J. Udaya Prakash, P. Maheandera Prabu, V. Perumal, and G. Kalusuraman, "Tribological behavior and surface characterization of gray cast iron-EN31 steel under lubricated sliding conditions," *Journal of Nanomaterials*, vol. 2021, Article ID 7725959, 9 pages, 2021.

[24] P. Sivaprakasam, G. Elias, P. M. Prabu, and P. Balasubramani, "Experimental investigations on wear properties of AlTiN coated 316LVM stainless steel," *Materials Today: Proceedings*, vol. 33, pp. 3470–3474, 2020.

[25] P. Sivaprakasam, A. Kirubel, G. Elias, P. Maheandera Prabu, and P. Balasubramani, "Mathematical modeling and analysis of wear behavior of AlTiN coating on titanium alloy (Ti-6Al-4V)," *Advances in Materials Science and Engineering*, vol. 2021, 9 pages, 2021.